SCIENTIFIC REPORTS
nature research

OPEN

Low-pressure-responsive heat-storage ceramics for automobiles

Shin-ichi Ohkoshi[1], Hiroko Tokoro[1,2], Kosuke Nakagawa[1], Marie Yoshikiyo[1], Fangda Jia[1] & Asuka Namai[1]

Received: 27 May 2019
Accepted: 24 August 2019
Published online: 18 September 2019

The accumulated heat energy of a heat-storage material is typically released over time. If a heat-storage material could preserve its accumulated heat energy for a prolonged period, the applicability of such materials would be expanded greatly. Herein we report a newly fabricated heat-storage material that can store latent heat energy for a long period and release the heat energy upon demand by applying an extremely low pressure. This material is a block-type lambda trititanium pentoxide (block-type λ-Ti_3O_5). The block-type λ-phase accumulates a large heat energy of 237 kJ L^{-1} and exhibits a pressure-induced phase transition to beta trititanium pentoxide. The pressure-induced phase transition occurs by applying only several tens of bars, and half of the fraction transforms by 7 MPa (70 bar). Such a *low-pressure-responsive heat-storage ceramic* is effective to reuse excessive heat in automobiles or waste heat at industrial factories.

Automobiles, such as cars, trucks, and buses gain power using heat energy from burning fuel in an engine. Upon initiating the engine, an automobile consumes energy to warm the internal system to the appropriate temperature in order to start driving. On the other hand, excessive heat energy is generated and released into the atmosphere while driving. Fuel consumption would be reduced if this excessive heat energy could be used when restarting a car. Materials capable of accumulating heat energy, which are known as heat-storage materials, are classified into two categories: sensible heat-storage materials and solid–liquid latent heat-storage materials. The former includes bricks and concrete[1,2], while the latter includes water, paraffin, and polyethylene glycol[3,4]. Regardless of the category, these materials release their accumulated heat energy over time. From this viewpoint, we focus on lambda trititanium pentoxide[5,6], which is one of the external-stimuli-induced phase transition materials[7–23]. The accumulated energy in lambda trititanium oxide can be stored and released by an external pressure[24]. Such a heat-storage behavior cannot be observed in typical pressure-induced phase transitions[25–36]. Therefore, this material suggests potential applications in the industry[37,38]. More preferably, the pressure to extract the accumulated heat energy is desired to be less than 10 MPa (100 bar). Herein we develop an extremely low-pressure-responsive heat-storage ceramic composed of block-type λ-Ti_3O_5. This paper describes the material synthesis, crystal structure, and morphology of block-type λ-Ti_3O_5. Additionally, the low-pressure-induced phase transition, heat-storage process, thermal hysteresis loop, and the mechanism of the observed phenomenon in this material are reported.

Results and Discussion

Material, crystal structure, and morphology. The target material was prepared by sintering the precursor rutile-type TiO_2 at 1300 °C for 2 hours under a hydrogen atmosphere. The detail synthesis is described in the Methods section (Fig. S1). Elemental analysis by X-ray fluorescence (XRF) suggests that the formula of the obtained sample is $Ti_{3.00}O_{5.00}$ (Calc.: Ti 64.2%, O 35.8%; Found: Ti 64.1%, O 35.9%). The powder X-ray diffraction (PXRD) pattern with Rietveld analysis indicates a monoclinic crystal structure in the *C*2/*m* space group with lattice parameters of $a = 9.8256(2)$ Å, $b = 3.78889(4)$ Å, $c = 9.9723(2)$ Å, and $\beta = 91.2751(14)°$. These features correspond to a crystal structure of λ-Ti_3O_5 (Fig. 1a,b, Table S1)[5]. In addition, the β-phase is included as a minor phase (monoclinic, *C*2/*m*, $a = 9.7659(3)$ Å, $b = 3.79907(7)$ Å, $c = 9.4445(3)$ Å, $\beta = 91.533(3)°$). The morphology of the sample was investigated by transmission electron microscopy (TEM). The sample is comprised of block-shaped crystals of sub-micrometer length on a side (Figs 1c and S2). This crystal size is remarkably large compared to previously reported samples. According to the morphology of the primary particles, we call the present material *block-type lambda trititanium pentoxide* (block-type λ-Ti_3O_5).

[1]Department of Chemistry, School of Science, The University of Tokyo, 7-3-1 Hongo, Bunkyo-ku, Tokyo, 113-0033, Japan. [2]Division of Materials Science, Faculty of Pure and Applied Sciences, University of Tsukuba, 1-1-1 Tennodai, Tsukuba, Ibaraki, 305-8573, Japan. Correspondence and requests for materials should be addressed to S.O. (email: ohkoshi@chem.s.u-tokyo.ac.jp)

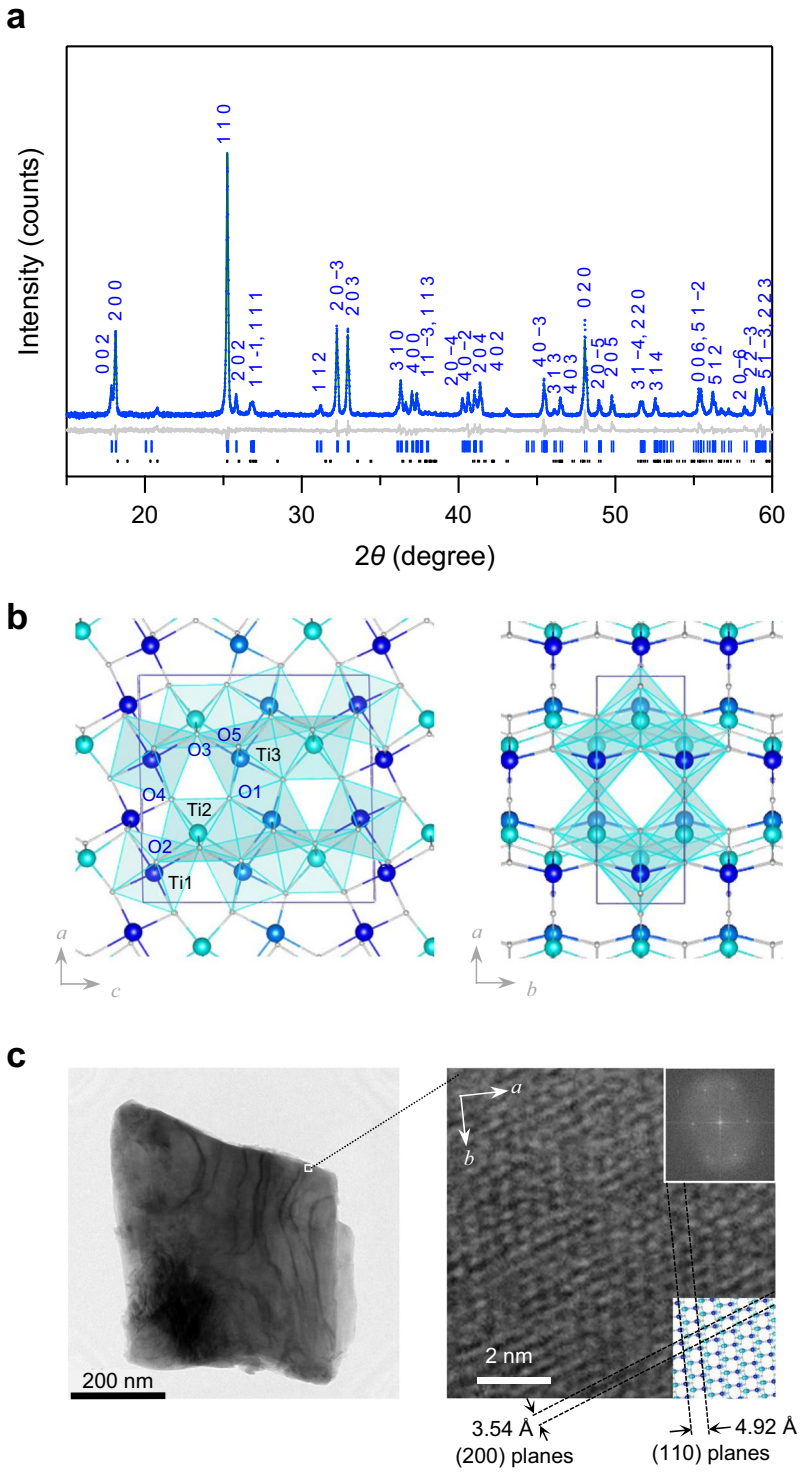

Figure 1. Morphology and crystal structure of block-type λ-Ti_3O_5. (**a**) XRPD pattern and Rietveld analysis of block-type λ-Ti_3O_5. (**b**) Crystal structure of block-type λ-Ti_3O_5 viewed along the *b*-axis (left) and *c*-axis (right). (**c**) TEM image of block-type λ-Ti_3O_5 (left) and enlarged figure of the TEM image with clear lattice fringes (right). Insets show the Fourier transform image (upper) and the atomic positions of the corresponding lattices (lower).

Release of heat energy by applying pressure to the λ-phase. The pressure effect on block-type λ-Ti_3O_5 was investigated by PXRD measurements after applying an external pressure (*P*) of 2.5, 5, 7.5, 10, 12.5, 15, 30, 45, 60, 230, or 600 MPa (Figs 2a and S3). As the pressure increases, the phase fraction of λ-Ti_3O_5 decreases while that of β-Ti_3O_5 increases (Fig. 2b). Above 30 MPa, the phase fractions show constant values. The transition pressure ($P_{1/2}$), which is where the phase fractions of λ-Ti_3O_5 and β-Ti_3O_5 are equal, is 7 MPa.

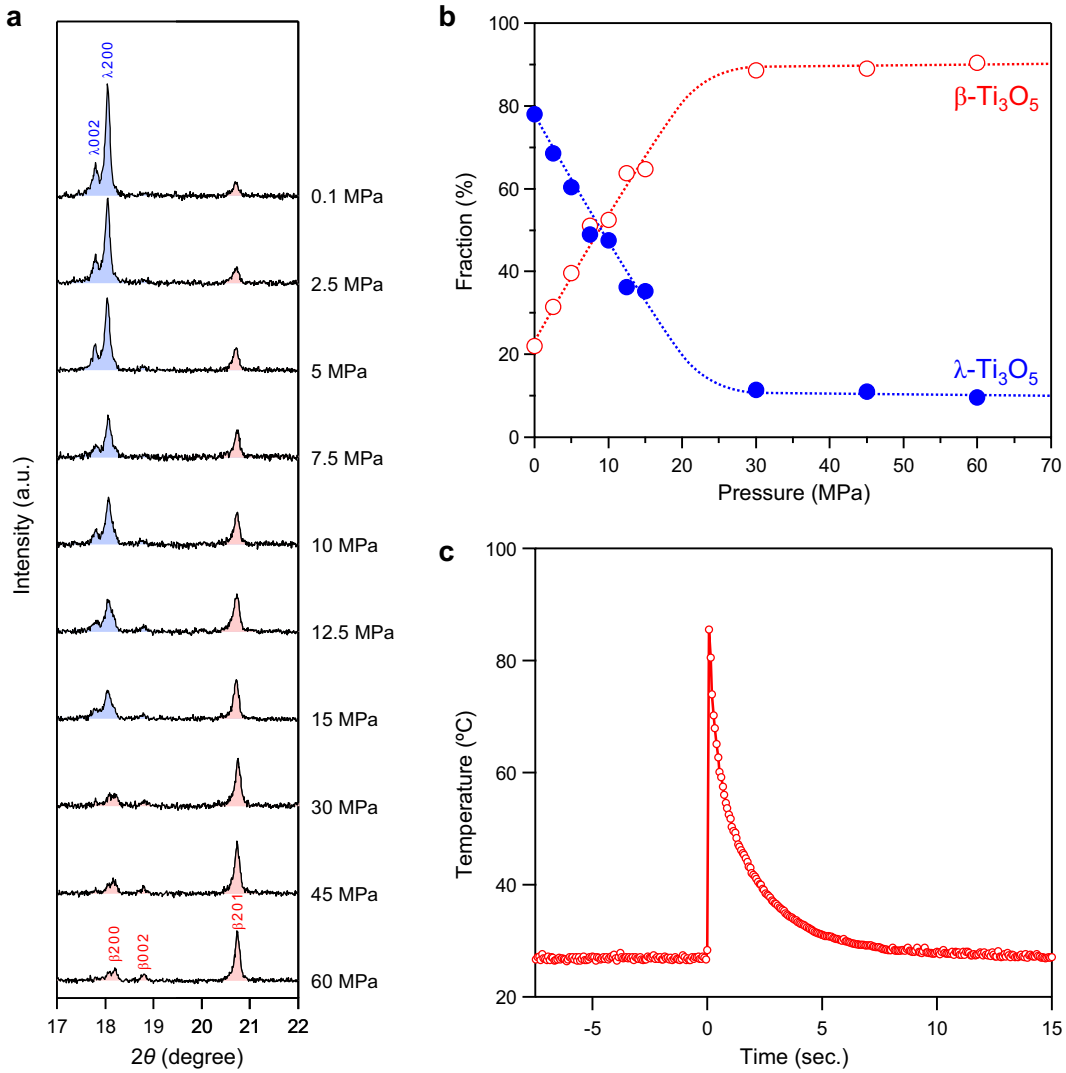

Figure 2. Pressure evolution of the phase fractions and pressure-induced heat release of block-type λ-Ti_3O_5. (**a**) Pressure evolution of the PXRD pattern. Blue and red indicate the peaks assigned to λ-Ti_3O_5 and β-Ti_3O_5, respectively. (**b**) Phase fractions of block-type λ-Ti_3O_5 (blue) and β-Ti_3O_5 (red) versus applied pressure. (**c**) Time dependence of the sample temperature on applying pressure as observed by thermography. Pressure is applied to the sample at $t = 0$.

Thermograms before and after a pressure application. We visually measured the temperature change of the sample during a pressure-induced phase transition using thermography (Fig. 2c, Supplementary Movie S1). Pressure was applied by hitting the sample using a hammer. Initially, the temperature is 26.8 °C, and the thermal image is blue. Hitting the sample with a hammer instantly changes the thermal image color to white, which successively turns red, orange, yellow, green, and then back to blue (Fig. 3). The maximum temperature of the white area is 85.5 °C, indicating a temperature increase of 60 °C. The sample temperature reaches a maximum value in less than 67 ms after applying pressure, indicating that the heat energy is immediately released upon applying pressure. Then the temperature exponentially decreases with a decay time of 1.7 s.

We carried out the estimation of the pressure-released heat energy using thermography. Based on the heat capacity versus temperature curve of β-phase[24], and by considering the temperature increase and the conversion ratio after hitting the sample with a hammer, the pressure-released energy was estimated to be $235 \pm 7\,kJ\,L^{-1}$. The details of the estimation process are described in Supplementary Section 6.

Heat-storage process from the β- to λ-phase. The heat-storage temperature and accumulated heat energy were measured with a differential scanning calorimeter (DSC). For the measurement, the pressure-produced β-phase was used. In the initial heating process from room temperature to 600 K, an endothermic peak (i.e., heat-storage peak) is observed at 471 K (198 °C). Analyses of the DSC curve shows that the accumulated heat energy is $237\,kJ\,L^{-1}$ (Fig. 4a). Conversely, in the cooling process from 600 K to 300 K, an exothermic peak (i.e., heat-release peak) is not observed. These data indicate that λ-Ti_3O_5 stores the latent heat energy of $237\,kJ\,L^{-1}$.

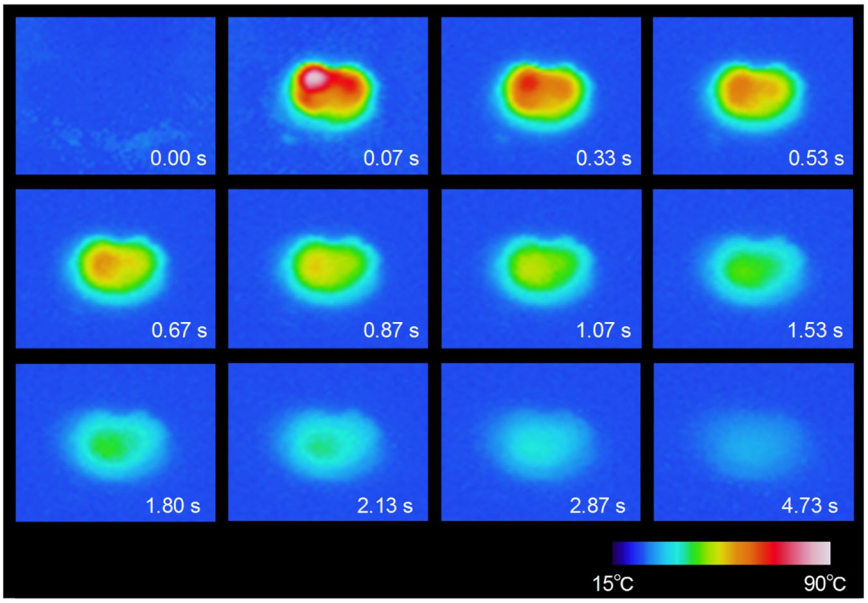

Figure 3. Time evolution of the thermographic image on applying pressure to block-type λ-Ti_3O_5. Snapshots taken from the thermogram of the sample on applying pressure as observed by thermography. Pressure is applied to the sample at $t = 0$. The sample temperature reached a maximum of 85.5 °C.

Thermal hysteresis loop of the phase transition between the β- and λ-phases. To investigate the origin of such a low pressure–induced phase transition, we measured the temperature dependence of the magnetic susceptibility (χ) of block-type λ-Ti_3O_5 using a superconducting quantum interference device (SQUID) magnetometer (Figs 4b and S4). In the cooling process from 600 K, the χ value remains nearly constant around 0.0003 emu per Ti atom, gradually decreases below 150 K, but rapidly increases below 30 K. In the heating process from 2 K to 190 K, the χ values are the same as those in the cooling process. In the heating process around 190 K, the χ value begins to diverge; it takes lower values but abruptly increases at 455 K until it returns to the original values. A thermal hysteresis loop is observed with a branch point in the low temperature region (T_L) of 190 K and a closing point in the high temperature region (T_H) of 455 K. The temperature width of the thermal hysteresis ($\Delta T \equiv T_H - T_L$) is 265 K. Such a thermal hysteresis loop has not been observed in the previous λ-Ti_3O_5. It should be noted that the χ value of ~0.0003 emu per Ti atom in the cooling process indicates Pauli paramagnetism. The gradual decrease below 150 K is due to the spin–orbital interaction of the Ti^{3+} ions, while the increase below 30 K is attributed to the Curie paramagnetic component due to lattice defects.

Mechanism of the appearance of thermal hysteresis loop and low pressure–induced heat energy release. Next we considered the origin of the thermal hysteresis between the λ- and β-phases and the phase transition with an extremely weak pressure using thermodynamic analysis based on the Slichter and Drickamer mean-field model (SD model) (see Methods)[39]. In the SD model, the Gibbs free energy (G) of the system is described as $G = x\Delta H + \gamma x(1 - x) + T\{R[x \ln x + (1 - x)\ln(1 - x)] - x\Delta S\} + G_\beta$ with the Gibbs free energy of β-phase (G_β) as the standard, and the interaction parameter (γ) between the λ- and β-phases related to the elastic interactions inside the crystal is defined by $\gamma = \gamma_a + \gamma_b(T) + \gamma_c(P)$. From the result of the DSC measurement, the transition enthalpy (ΔH) is 13.7 kJ mol^{-1}. When the transition entropy (ΔS) and interaction parameters are set as a particular combination of values, the SD model calculation well reproduces the observed thermal hysteresis; i.e., the phase transitions of β-phase → λ-phase and λ-phase → β-phase occur at T_L of 194 K and T_H of 458 K, respectively, at a pressure of 0.1 MPa (1 bar) (Fig. S5a, black line). Hence, the thermal hysteresis loop appears due to the existence of the energy barrier between two bistable phases with close energy states. Furthermore, by assuming the γ value has a distribution due to the inhomogeneity of the primary crystal size, the SD model calculation well reproduces the observed hysteresis loop as shown in Fig. 5a, where the transition in the cooling process is gradual and that in the heating process is abrupt.

Next, we calculated the pressure dependence of the λ-Ti_3O_5 phase fraction. Applying pressure to the system causes the energy barrier to disappear and induces a phase transition from λ-Ti_3O_5 to β-Ti_3O_5 (Fig. 5b). Figure S5b shows the x vs. T plots at $P = 30$ MPa. The pressure dependence of x shows a threshold in the pressure-induced phase transition. By considering the distribution of the γ value (Fig. S5c), a gradual pressure-induced phase transition as in Fig. 2b is well reproduced (Fig. 5c).

Conclusion

Herein we report a newly developed heat-storage ceramic based on block-type λ-Ti_3O_5, which preserves the heat energy for a long period and shows a low pressure–induced heat energy release. Block-type λ-Ti_3O_5 accumulates a large latent heat energy of 237 kJ L^{-1}, and the accumulated heat energy can be extracted by applying

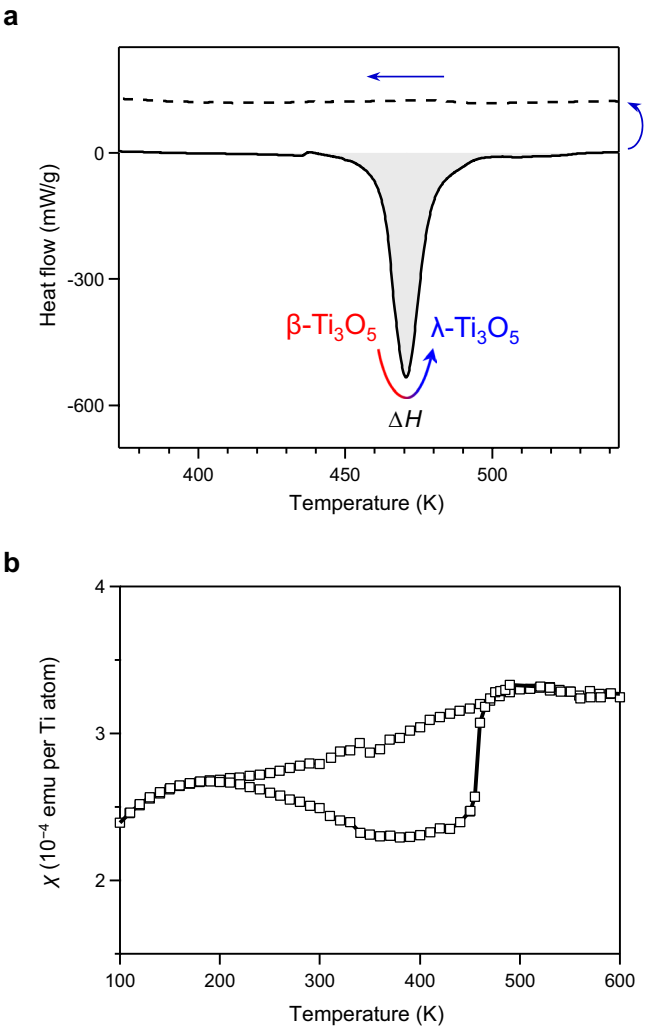

Figure 4. Heat-storage properties and thermal hysteresis loop of block-type λ-Ti_3O_5. (**a**) DSC chart of block-type λ-Ti_3O_5 with increasing temperature (solid line) and decreasing temperature (dotted line). (**b**) Temperature dependence of the magnetic susceptibility (χ) of block-type λ-Ti_3O_5.

an extremely weak pressure of only several MPa with a $P_{1/2}$ value of 7 MPa. For example, the pressure of a compressed gas cylinder is in the range from 12 to 30 MPa[40], suggesting that the present material could be triggered using a gas cylinder. The long-term heat-storage property of block-type λ-Ti_3O_5 and its release of accumulated heat energy by low pressure originate from the bistability (λ-phase and β-phase) of the present material and the existence of an energy barrier between the two phases. Due to the energy barrier, block-type λ-Ti_3O_5 exhibits one of the largest thermal hysteresis loops among condensed matter with a ΔT value of 265 K. Because the energy barrier disappears under weak pressure, the λ-phase transforms into the β-phase and releases the accumulated latent heat energy, which is comparable to the latent heat energies of solid–liquid phase-transition materials, e.g., water (320 kJ L^{-1}), paraffin (140 kJ L^{-1}), and polyethylene glycol (165 kJ L^{-1}). The energy barrier is attributed to the elastic interaction within the material. The behaviors of the temperature dependence and pressure dependence of block-type λ-Ti_3O_5 are well reproduced by thermodynamic calculations. From the viewpoint of automobile applications, transition pressures below 10 MPa are preferable. Therefore, the present heat-storage ceramic should be useful in automobile components near engines and mufflers (Fig. 6)[37,38], since the heat-storage ceramic can warm the cooled internal system when restarting the automobile. Additionally, an example of other possible applications is solar power plants. In solar power plants, nitrates have been used in the heat storage tanks. Since the present material has both properties of long-term latent heat storage and sensible heat storage, it is expected to be useful for the heat storage system at solar power plants (Fig. S6).

Methods

Physical measurements. Elemental analysis of the prepared sample was performed using X-ray fluorescence spectroscopy (Rigaku, ZSX PrimusII). TEM measurements were conducted using a JEOL JEM-2000EXII and JEM-4000FXII. The XRD measurements were conducted by a Rigaku Ultima IV with Cu Kα radiation ($\lambda = 1.5418$ Å). Rietveld analyses were performed by the RIETAN-FP program. The magnetic properties were

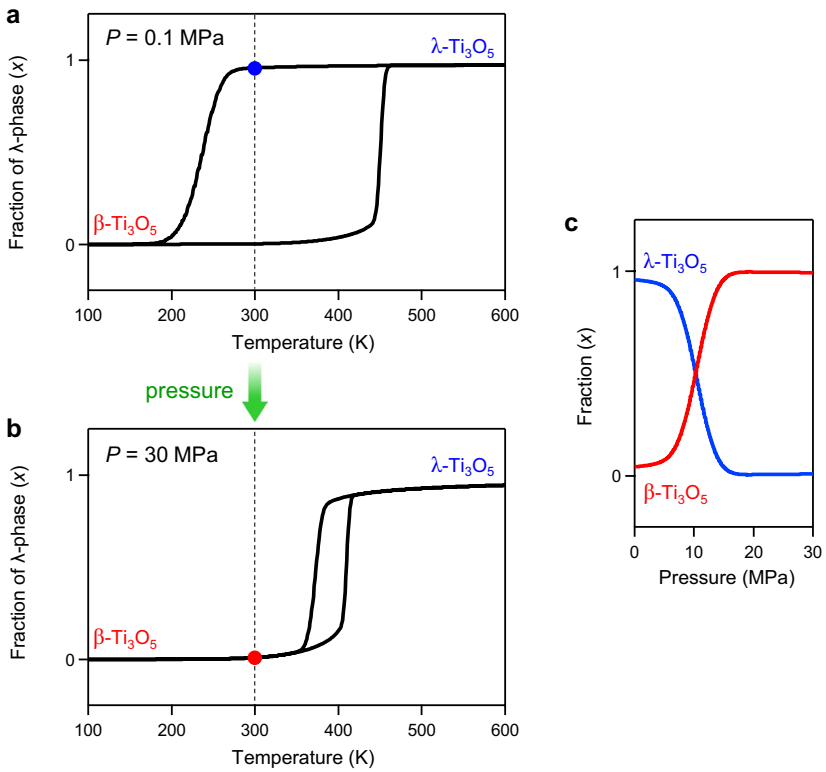

Figure 5. Mechanism of the pressure-induced phase transition based on the Slichter-Drickamer mean-field model. (**a**,**b**) Calculated λ-phase fraction (x) versus temperature curves at $P = 0.1$ MPa (**a**) and 30 MPa (**b**). Calculations were performed for the cooling process and the heating process under the conditions of $\Delta H = 13.7\,\mathrm{kJ\,mol^{-1}}$, $\Delta S = 34.6\,\mathrm{J\,K^{-1}\,mol^{-1}}$, $\gamma_b = -2.4\,\mathrm{J\,K^{-1}\,mol^{-1}}$, and $\gamma_c = -0.12\,\mathrm{kJ\,MPa^{-1}\,mol^{-1}}$, while assuming the γ_a value has a normal distribution centered at $12.88\,\mathrm{kJ\,mol^{-1}}$ with a standard deviation of $0.3\,\mathrm{kJ\,mol^{-1}}$. (**c**) Calculated λ-phase and β-phase fractions versus pressure at 300 K.

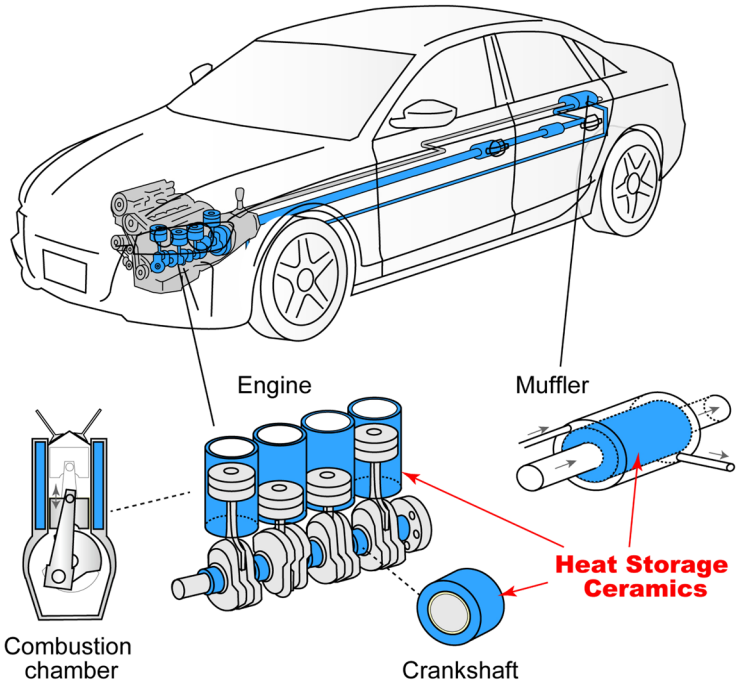

Figure 6. Possible applications of block-type λ-Ti_3O_5 for automobiles. Schematic image of where block-type λ-Ti_3O_5 could be applied as a heat-storage material in an automobile. Blue areas indicate the possible components to use the heat-storage material: combustion chamber, crankshaft, and muffler.

measured using a superconducting quantum interference device (SQUID) magnetometer (Quantum Design, MPMS 7). DSC was performed on a Rigaku DSC 8230.

Thermodynamic analysis. In the Slichter and Drickamer mean-field model, the Gibbs free energy of the system is described as $G = x\Delta H + \gamma x(1-x) + T\{R[x\ln x + (1-x)\ln(1-x)] - x\Delta S\} + G_\beta$, where x is the ratio of the λ-phase. ΔH and ΔS are the transition enthalpy and transition entropy for the transition between the λ- and the β-phases, respectively. γ is the interaction parameter between the λ- and β-phases. G_β is the Gibbs free energy of the β-phase, which is set as the origin of the energies, and R is the gas constant. The γ value depends on the temperature and pressure; *i.e.*, $\gamma = \gamma_a + \gamma_b(T) + \gamma_c(P)$. The observed phase transition is due to the metal–semiconductor phase transition between charge-delocalized λ-Ti_3O_5 and charge-localized β-Ti_3O_5, which are regarded as $Ti(1)^{3.3+}$–$Ti(2)^{3.3+}$–$Ti(3)^{3.3+}$ and $Ti(1)^{3.0+}$–$Ti(2)^{3.7+}$–$Ti(3)^{3.3+}$, respectively. From the DSC measurement result, the ΔH value is 13.7 kJ mol^{-1}. When the ΔS value and the interaction parameters are set as follows: $\Delta S = 34.6$ J K^{-1} mol^{-1}, $\gamma_a = 13.48$ kJ mol^{-1}, $\gamma_b = -2.4$ J K^{-1} mol^{-1}, and $\gamma_c = -0.12$ kJ MPa^{-1} mol^{-1}, the SD model calculations indicated thermal hysteresis loops as shown in Fig. S5a,b (black lines). Furthermore, by assuming that the γ_a value has a normal distribution centered at 12.88 kJ mol^{-1} with a standard deviation of 0.3 kJ mol^{-1} (Fig. S5c), the SD model calculation qualitatively reproduces the observed thermal hysteresis loop. The pressure dependence of x was also calculated using the same parameters.

Data Availability

All data are available upon reasonable request from the corresponding authors.

References

1. Nahas, M. K. & Constable, F. H. Thermal conductivity of mud brick. *Nature* **142**, 837 (1938).
2. Al-Jabri, K. S., Hago, A. W., Al-Nuaimi, A. S. & Al-Saidy, A. H. Concrete blocks for thermal insulation in hot climate. *Cem. Concr. Res.* **35**, 1472–1479 (2005).
3. Farid, M. M., Khudhair, A. M., Razack, S. A. K. & Al-Hallaj, S. A review on phase change energy storage: materials and applications. *Energ. Convers. Manage.* **45**, 1597–1615 (2004).
4. Sharma, A., Tyagi, V. V., Chen, C. R. & Buddhi, D. Review on thermal energy storage with phase change materials and applications. *Renew. Sust. Energ. Rev.* **13**, 318–345 (2009).
5. Ohkoshi, S. *et al*. Synthesis of a metal oxide with a room-temperature photoreversible phase transition. *Nature Chemistry* **2**, 539–545 (2010).
6. Makiura, R. *et al*. Nanoscale effects on the stability of the λ-Ti_3O_5 polymorph. *Chem. Asian J.* **6**, 1886–1890 (2011).
7. Kolobov, A. V. *et al*. Understanding the phase-change mechanism of rewritable optical media. *Nature Materials* **3**, 703–708 (2004).
8. Wuttig, M. & Yamada, N. Phase-change materials for rewriteable data storage. *Nature Materials* **6**, 824–832 (2007).
9. Heintze, E. *et al*. Dynamic control of magnetic nanowires by light-induced domain-wall kickoffs. *Nature Materials* **12**, 202–206 (2013).
10. Fiebig, M., Miyano, K., Tomioka, Y. & Tokura, Y. Visualization of the local insulator–metal transition in $Pr_{0.7}Ca_{0.3}MnO_3$. *Science* **280**, 1925–1928 (1998).
11. Gütlich, P., Gaspar, A. B. & Garcia, Y. Spin state switching in iron coordination compounds. *Beilstein J. Org. Chem.* **9**, 342–391 (2013).
12. Létard, J. F. *et al*. Light induced excited pair spin state in an iron(II) binuclear spin-crossover compound. *J. Am. Chem. Soc.* **121**, 10630–10631 (1999).
13. Ohkoshi, S. *et al*. 90-degree optical switching of output second-harmonic light in chiral photomagnet. *Nature Photonics* **8**, 65–71 (2014).
14. Ohkoshi, S., Imoto, K., Tsunobuchi, Y., Takano, S. & Tokoro, H. Light-induced spin-crossover magnet. *Nature Chemistry* **3**, 564–569 (2011).
15. Nasu, K. Relaxations of Excited States and Photo-Induced Structural Phase Transitions (Springer, Berlin, 1997).
16. Decurtins, S., Gütlich, P., Köhler, C. P., Spiering, H. & Hauser, A. Light-induced excited spin state trapping in a transition-metal complex: The hexa-1-propyltetrazole-iron (II) tetrafluoroborate spin-crossover system. *Chem. Phys. Lett.* **105**, 1–4 (1984).
17. Irie, M., Fukaminato, T., Sasaki, T., Tamai, N. & Kawai, T. A digital fluorescent molecular photoswitch. *Nature* **420**, 759–760 (2002).
18. Koshihara, S., Tokura, Y., Mitani, T., Saito, G. & Koda, T. Photoinduced valence instability in the organic molecular compound tetrathiafulvalence-p-chloranil (TTF-CA). *Phys. Rev. B* **42**, 6853–6856 (1990).
19. Collet, E. *et al*. Laser-induced ferroelectric structural order in an organic charge-transfer crystal. *Science* **300**, 612–615 (2003).
20. Ohkoshi, S. & Tokoro, H. Photomagnetism in cyano-bridged bimetal assemblies. *Acc. Chem. Res.* **45**, 1749–1758 (2012).
21. Herrera, J. M. *et al*. Reversible photoinduced magnetic properties in the heptanuclear complex $[Mo^{IV}(CN)_2(CN\text{-}CuL)_6]^{8+}$: A photomagnetic high-spin molecule. *Angew. Chem. Int. Ed.* **43**, 5468–5471 (2004).
22. Margadonna, S., Prassides, K. & Fitch, A. N. Large lattice responses in a mixed-valence Prussian blue analogue owing to electronic and spin transitions induced by X-ray irradiation. *Angew. Chem. Int. Ed.* **43**, 6316–6319 (2004).
23. Nayak, A. P. *et al*. Pressure-induced semiconducting to metallic transition in multilayered molybdenum disulphide. *Nature Communications* **5**, 3731/1–9 (2014).
24. Tokoro, H. *et al*. External stimulation-controllable heat-storage ceramics. *Nature Communications* **6**, 7037/1–8 (2015).
25. Sato, H. *et al*. Baddeleyite-type high-pressure phase of TiO_2. *Science* **251**, 786–788 (1991).
26. Huang, L., Durandurdu, M. & Kieffer, J. Transformation pathways of silica under high pressure. *Nature Materials* **5**, 977–981 (2006).
27. Karzel, H. *et al*. Lattice dynamics and hyperfine interactions in ZnO and ZnSe at high external pressures. *Phys. Rev. B* **53**, 11425–11438 (1996).
28. Lipinska-Kalita, K. E., Kalita, P. E., Hemmers, O. A. & Hartmann, T. Equation of state of gallium oxide to 70 GPa: Comparison of quasihydrostatic and nonhydrostatic compression. *Phys. Rev. B* **77**, 094123 (2008).
29. Azuma, M. *et al*. Colossal negative thermal expansion in $BiNiO_3$ induced by intermetallic charge transfer. *Nature Communications* **2**, 347 (2011).
30. Ahart, M. *et al*. Origin of morphotropic phase boundaries in ferroelectrics. *Nature* **451**, 545–548 (2008).
31. Medvedev, S. *et al*. Electronic and magnetic phase diagram of β-$Fe_{1.01}Se$ with superconductivity at 36.7 K under pressure. *Nature Materials* **8**, 630–633 (2009).
32. Tolbert, S. H. & Alivisatos, A. P. Size dependence of a first order solid-solid phase transition: The wurtzite to rock salt transformation in CdSe nanocrystals. *Science* **265**, 373–376 (1994).
33. Hanfland, M., Syassen, K., Christensen, N. E. & Novikov, D. L. New high-pressure phases of lithium. *Nature* **408**, 174–178 (2000).
34. McMahon, M. I., Nelmes, R. J., Allan, D. R., Belmonte, S. A. & Bovornratanaraks, T. Observation of a simple-cubic phase of GaAs with a 16-atom basis (SC16). *Phys. Rev. Lett.* **80**, 5564–5567 (1998).

35. Mujica, A., Rubio, A., Muñoz, A. & Needs, R. J. High-pressure phases of group-IV, III-V, and II-VI compounds. *Rev. Mod. Phys.* **75**, 863–912 (2003).
36. Takabayashi, Y. *et al*. The disorder-free non-BCS superconductor Cs_3C_{60} emerges from an antiferromagnetic insulator parent state. *Science* **323**, 1585–1590 (2009).
37. Honda, A. & Ohkoshi, S. Internal combustion engine. JP6426658 patent (2018).
38. Honda, A. & Ohkoshi, S. Internal combustion engine. DE102017109005 patent (2018).
39. Slichter, C. P. & Drickamer, H. G. Pressure-induced electronic changes in compounds of iron. *J. Chem. Phys.* **56**, 2142–2160 (1972).
40. Department of Labour, Wellington, New Zealand. Guide to gas cylinders (1992).

Acknowledgements

The present research was supported in part by a JSPS Grant-in-Aid for Specially Promoted Research (Grant Number 15H05697) and JSPS Grant-in-Aid for Scientific Research (Grant Number 17H06367). We also recognize the Cryogenic Research Center, The University of Tokyo, and Nanotechnology Platform, which are supported by MEXT.

Author Contributions

S.O. designed and coordinated this study, contributed to all measurements and calculations, and wrote the paper. H.T. conducted the thermodynamic calculations. K.N. conducted the elemental analyses, PXRD measurements, and SQUID measurements. M.Y. contributed to the sample preparation, carried out the TEM observations, and partially wrote the paper. F.J. carried out the pressure dependence experiments and thermodynamic calculations. A.N. conducted Rietveld analyses, contributed to the thermodynamic calculations, and prepared the figures.

Additional Information

Supplementary information accompanies this paper at https://doi.org/10.1038/s41598-019-49690-0.

Competing Interests: The authors declare no competing interests.

Publisher's note: Springer Nature remains neutral with regard to jurisdictional claims in published maps and institutional affiliations.